

## 論文内容の要旨

### Structural Study on Prorocentrol, a Polyene-Polyol Compound from an Epiphytic Dinoflagellate *Prorocentrum hoffmannianum*

(付着性渦鞭毛藻 *Prorocentrum hoffmannianum* 由来ポリエンポリオール化合物  
prorocentrol の構造研究)

菅原 孝太郎

Dinoflagellates, a type of unicellular phytoplankton, are a rich source of secondary metabolites, which fascinates us a lot for their structural features and potent biological activities. From genus *Prorocentrum*, okadaic acid (OA) was confirmed as the causative substance of diarrhetic shellfish poisoning and later turned out to be a potent inhibitor of protein phosphatase 2A. In addition, genus *Prorocentrum* produces hoffmannioidide, prorocentrolides, and spiro-prorocentrimine, having diverse structural features as polyether carboxylic acid, macrolactones, and cyclicimines.

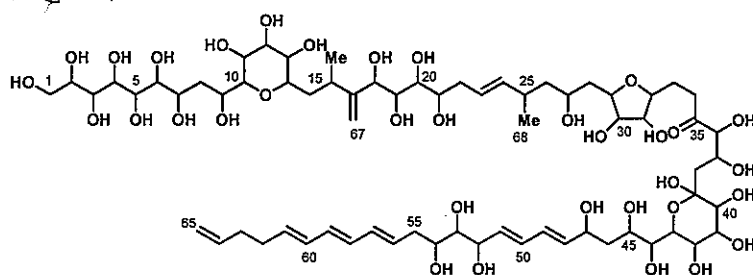


Fig. 1. Planar structure of prorocentrol

During our continuing search for new secondary metabolites from marine dinoflagellates, we have identified a new polyene-polyol with a molecular weight of 1474, named prorocentrol, in the cell extracts of *Prorocentrum hoffmannianum*. Prorocentrol possesses unique structural features such as diene, triene, hemiacetal, ketone moieties, and 30 hydroxy groups. With regards to the biological activities, prorocentrol inhibits growth of murine leukemia cells P388 at 15  $\mu\text{g/mL}$  and diatom *Nitzschia* sp. at 50  $\mu\text{g/mL}$ . In addition, inhibition of spore formation against the fungus *Aspergillus niger* was observed at 100  $\mu\text{g/disc}$ .

Structural elucidation of prorocentrol has not been completed because of a ketone-hemiacetal tautomerism during the course of NMR measurements. In this research, to obtain a single tautomer for NMR analysis was the

first target in order to investigate its stereochemistry related to further biological properties.

### Isolation and planar structure of prorocentrol

The dinoflagellate *P. hoffmannianum* was grown for 30-45 days at 25 °C in a seawater medium enriched with *f/2* nutrients. The cultured cells were harvested by centrifugation and then extracted with methanol. The extracts were subjected to 4 steps of biphasic partition as shown in Fig. 2. Since the 1-butanol extracts contained a lot of okadaic acid, this extract was partitioned between ethyl acetate and 0.15% acetic acid, resulting in effective removal of okadaic acid from prorocentrol. The 0.15% AcOH extracts were passed through an ODS column, HW-40(S) column, and finally purification using ODS MPLC afforded prorocentrol as colorless amorphous solid. During the above purification procedures, prorocentrol in eluates were monitored with a photodiode array detector at 271 nm and also by ion peak at 1497  $[M+Na]^+$  on MALDI-MS spectra.

The high resolution ESI-MS gave  $[M+Na]^+$  at  $m/z$  1497.7089 ( $\Delta -1.5$  mmu), and its molecular formula was deduced to be  $C_{68}H_{114}O_{34}$ . The UV and IR absorption spectra suggested the presence of conjugated diene ( $\lambda_{max}$  232 nm) and conjugated triene ( $\lambda_{max}$  260, 270 and 281 nm) chromophores, and hydroxy groups ( $\nu_{max}$  3365  $cm^{-1}$ ) and ketones ( $\nu_{max}$  1711  $cm^{-1}$ ). The  $^{13}C$ -NMR spectra in methanol- $d_4$  and DMF- $d_7$  were very complicated with more than 68 signals observed. This phenomenon is explained by the keto-enol tautomerism or ring opening acetal exchange at cyclic hemiacetal moiety. To resolve this problem, NMR measuring conditions such as solvents, pH, or temperature were examined to lead to the solvent system of pyridine- $d_5$ / $D_2O$  (6/1) giving simplified and improved spectrum at room temperature as shown in Fig. 3. Each signal around the acetal and the ketone was observed as a single peak in the  $^{13}C$ -NMR spectrum. All carbon signals were successfully assigned as 2 methyls, 12 aliphatic methylenes, 2 aliphatic methines, 1 oxymethylene, 33 oxymethines, 1 acetal, 16 olefins including one quaternary olefinic carbon, and 1 ketone. The numbers of hydroxy groups were estimated by measuring the  $^{13}C$ -NMR deuterium shift on the hydroxy bearing carbons between pyridine- $d_5$ / $H_2O$  (6/1) and pyridine- $d_5$ / $D_2O$  (6/1) solvent systems. Of all the monooxygenated carbons (64.6-100.9ppm), only the 5 oxymethines did not show the deuterium induced shift. These experimental data suggested prorocentrol possesses one hemiacetal and one ketone moieties as a major tautomer in this solvent system.

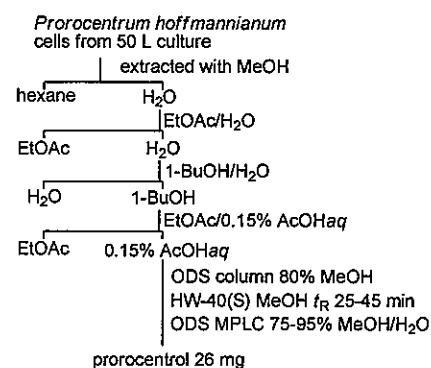


Fig. 2 Isolation scheme of prorocentrol

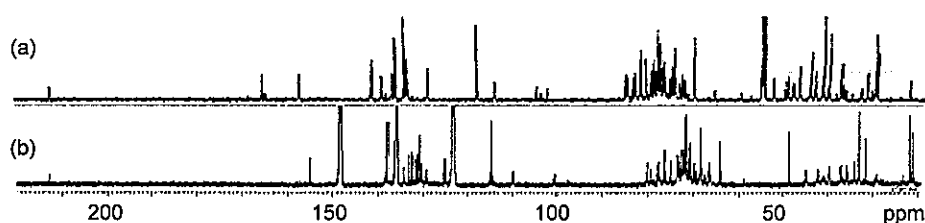


Fig. 3.  $^{13}C$ -NMR spectra of prorocentrol, (a): in methanol- $d_4$ , 125 MHz, (b): in py- $d_5$ / $D_2O$  6/1, 100 MHz.

A detailed analysis of the DQF-COSY, TOCSY, and HSQC-TOCSY spectra allowed us to elucidate 5 partial structures,  $C_1$ - $C_{15}$ ,  $C_{18}$ - $C_{34}$ ,  $C_{36}$ - $C_{38}$ ,  $C_{40}$ - $C_{41}$  and  $C_{42}$ - $C_{65}$ . In the HMBC spectra, a pair of hemiacetal and ketone signals was confirmed with corresponding correlation signals. This result supported the assignment of the one hemiacetal and one ketone structure as the major tautomer in pyridine- $d_5$ / $D_2O$  (6/1). In a similar way, two partial structures were connected to a quaternary olefinic carbon. The presence of tetrahydrofuran and tetrahydropyran rings was also confirmed.

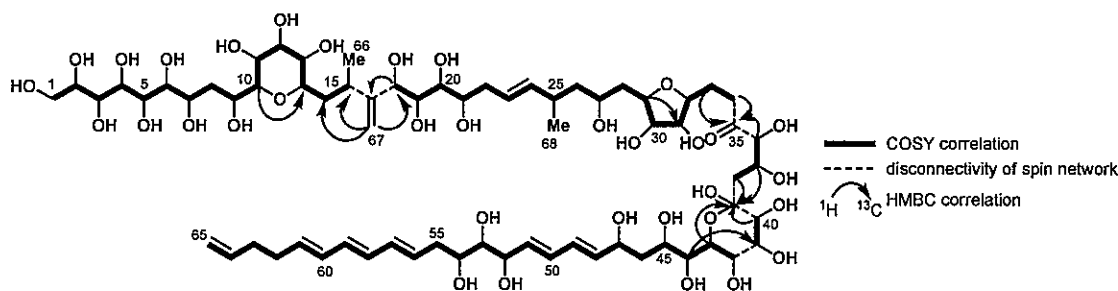


Fig. 4. NMR assignments of proocentrol.

### Relative configurational analysis on proocentrol

The relative configuration of the tetrahydropyran ring (C10–C14) of proocentrol was elucidated based on vicinal proton coupling constants and NOE correlations from E. COSY and 2D-NOESY spectra, respectively. Coupling constants and NOE correlations between protons on this ring suggested that this ring had a chair conformation as shown in Fig. 5. Although the relative configuration of the above cyclic structure was determined by the use of conventional NMR experiments, the problem was more complicated for contiguous polyol units on a long acyclic carbon chain. Therefore the author applied the JBCA (*J*-based configuration analysis), a method developed by Murata et. al. This method leads to the correct diastereomer of 1,2- or 1,3-methine systems through its major conformation based on estimated multi-bonded hetero and homonuclear coupling constants and thus indicated dihedral angles. For the C52–C55 portion,  $^3J_{H,H}$  and  $^{2,3}J_{C,H}$  values were obtained from E. COSY and HETLOC spectra, and dominant conformation and relative stereoconfiguration was shown as Newman projections and stereo projection in Fig. 6., respectively.

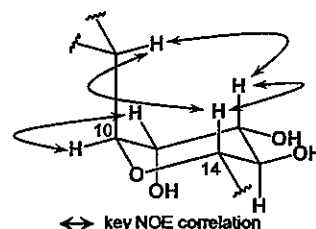


Fig. 5. Relative stereoconfiguration of C10–C14

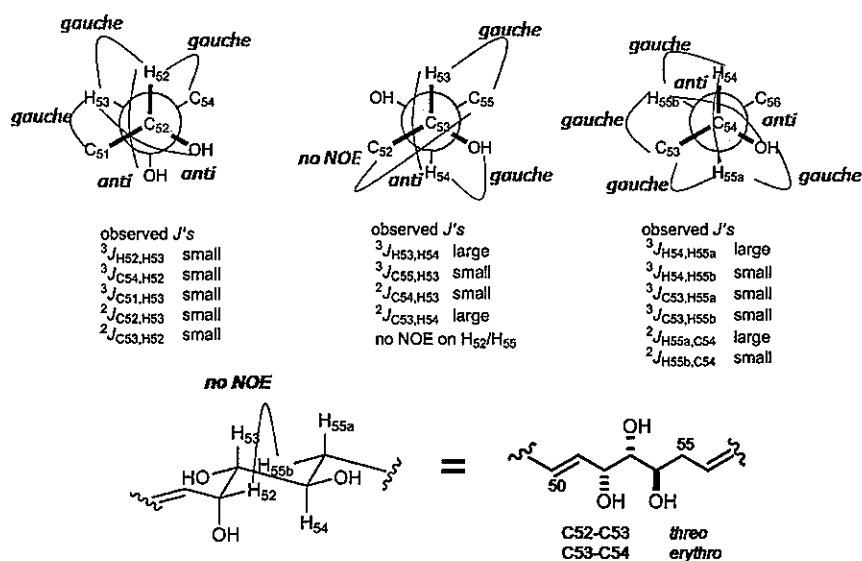


Fig. 6. Relative stereoconfiguration of C52–C53

Likewise, the longest polyol segment of proocentrol, C1–C9 portion was assigned by JBCA method as C2–C3, C3–C4, C4–C5, C5–C6, C6–C7, C7–C9, and C9–C10 into *erythro*, *threo*, *threo*, *threo*, *threo*, *syn*, and *threo* as shown in Fig. 7. By using JBCA method, relative stereoconfiguration at contiguous polyol segment of proocentrol in both termini was elucidated.

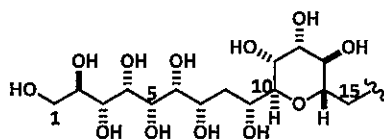


Fig. 7. Relative stereoconfiguration of C2 to C14

### Molecular interaction between prococontrol and okadaic acid

As mentioned in the isolation part, okadaic acid (OA) which should hardly be partitioned in water, was observed in  $^1\text{H-NMR}$  spectra of the prococontrol enriched fraction. Interestingly, some proton signals of okadaic acid were shifted under the coexistence of prococontrol.

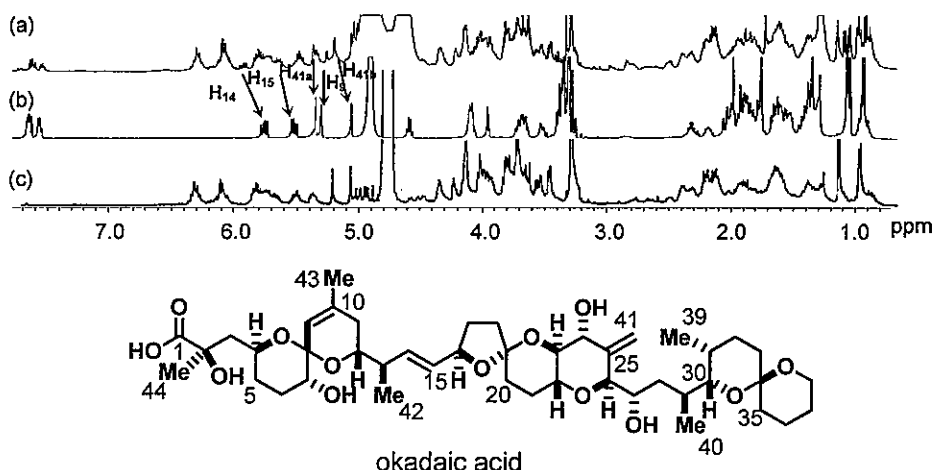


Fig. 8. Above: 500MHz  $^1\text{H-NMR}$  spectra in methanol- $d_4$ , (a) OA and prococontrol mixture, (b) OA, (c) prococontrol. Below: structure of okadaic acid (OA).

Considering the observed  $^1\text{H-NMR}$  signal shifts as shown in Fig. 8., specific association of prococontrol and okadaic acid was speculated. Since this phenomenon was suspected to affect the biological activity of okadaic acid, cytotoxicity of okadaic acid against P388 cells, which is 1000 times more potent than that of prococontrol, was examined under co-existence of OA/prococontrol. The obtained dose-response curves of a solution of OA /prococontrol 1/5 eq. were shown in Fig. 9. From this result, significant change in cytotoxicity of OA was not observed.

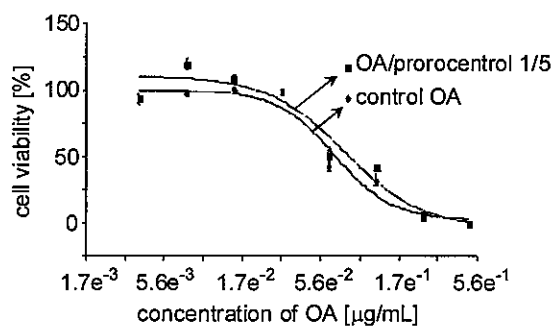


Fig. 9 Dose-response curve of cytotoxicity assay.